Zfp423 regulates Sonic hedgehog signaling via primary cilium function

Short title: *Zfp423* regulates cilium function in Shh signaling

Chen-Jei Hong[1,#a] and Bruce A. Hamilton1,*

[1]Department of Cellular & Molecular Medicine, Department of Medicine,
Moores UCSD Cancer Center, and Institute for Genomic Medicine
University of California, San Diego
La Jolla, CA 92093-0644

[#a] Current address: Neural Regeneration Laboratory, Neurological Institute, Taipei Veterans General Hospital, Taipei, Taiwan.

*Corresponding author
email: bah@ucsd.edu

ABSTRACT

Zfp423 encodes a 30-zinc finger transcription factor that intersects several canonical signaling pathways. *Zfp423* mutations result in ciliopathy-related phenotypes, including agenesis of the cerebellar vermis in mice and Joubert syndrome (JBTS19) and nephronophthisis (NPHP14) in humans. Unlike most ciliopathy genes, *Zfp423* encodes a nuclear protein and its developmental expression is complex, leading to alternative proposals for cellular mechanisms. Here we show that Zfp423 is expressed by cerebellar granule cell precursors, that loss of *Zfp423* in these precursors leads to cell-intrinsic reduction in proliferation, loss of response to Shh, and primary cilia abnormalities that include diminished translocation of both Smoothened and IFT88. Loss of Zfp423 alters expression of several genes encoding key cilium components, including increased expression of *Tulp3*. *Tulp3* is a direct binding target of Zfp423 and reducing the overexpression of Tulp3 in *Zfp423*-deficient cells suppresses Smoothened translocation defects. These results define *Zfp423* deficiency as a bona fide ciliopathy, acting upstream of Shh signaling, and indicate a mechanism intrinsic to granule cell precursors for the resulting cerebellar hypoplasia.

AUTHOR SUMMARY

Ciliopathies are a broad group of individually rare genetic disorders that share overlapping phenotypes and mutations in genes that make components of the primary cilium. Mutations in *ZNF423* are an exception. Patients and mouse models show characteristic hypoplasia of the cerebellar midline (Joubert syndrome), but the gene encodes a nuclear transcription factor. The mouse gene, *Zfp423*, is expressed in a dynamic developmental pattern, leaving the cellular mechanism for this brain malformation unresolved. One report suggested reduced Purkinje cell expression of Shh, a key mitogen for cerebellar granule cell precursors (GCPs) whose signal transduction occurs at the primary cilium, as the key event. We show that *Zfp423* mutants expressed normal Shh levels, but that *Zfp423*-depleted GCPs were unable to respond. Primary cilia on *Zfp423*-mutant GCPs in situ typically had a wider base and longer extension. ZNF423-depletion in a human cell culture model resulted in defective translocation of Smoothened, a key event in Shh signaling, and of the intraflagellar transport protein IFT88. RNA-Seq and RT-qPCR experiments identified known ciliopathy genes as potential conserved targets of *ZNF423* and *Zfp423*. One of these, *TULP3*, is both up-regulated in *ZNF423*/*Zfp423*-deficient cells and directly bound by Zfp423 in granule cell precursors. Reversing the overexpression of TULP3 in ZNF423-depleted human cell culture model reversed the defect in Smoothened translocation.

INTRODUCTION

Cerebellar granule cell precursors (GCPs) are both an important model for neuronal development and a site of clinically important developmental abnormalities. GCP proliferation is highly responsive to Purkinje cell-derived sonic hedgehog (Shh) over a wide dynamic range [1-3]. Increasing or decreasing developmental Shh signaling can alter GCP dynamics sufficiently to reshape the cerebellum [4]. Correspondingly, ligand-independent signaling through the Shh pathway is a common feature in medulloblastoma, the most common pediatric brain tumor [5-7], and the Shh signaling pathway is a focal point of therapeutic development [8-10]. Shh signaling at primary cilia, where multiple components are trafficked to create a focused signaling module [11-14], is required for GCP expansion [15]. How Shh signaling is integrated with other signals that impact GCP proliferation, migration, and differentiation is not fully understood.

Through alternative interactions with multiple signaling and transcriptional pathways, Zfp423 (and its human orthologue, ZNF423) is well positioned to integrate extracellular signals into a coherent developmental response. Zfp423 was first described (as Roaz) through inhibitory interaction with EBF (Olf1) helix–loop–helix transcription factors [16]. Zfp423 is also a coactivator for BMP-activated SMADs [17, 18], retinoic acid receptors [19, 20], and Notch intracellular domain [21]. Intriguingly, Zfp423 activities on EBF and ligand-activated factors appear to be mutually inhibitory, further suggesting an integrative network function. *ZNF423* also appears to be a target of some cancers and low expression in neuroblastoma [20] or epigenetic silencing by Polycomb repressive complex 2 in glioma [22] is associated with poor prognosis.

Zfp423-deficient mice have a variety of developmental defects, including fully penetrant loss of cerebellar vermis [23-25] and variable loss of cerebellar hemispheres dependent on modifier genes and other factors [26]. Zfp423-deficient animals are also

defective in forebrain development–including hypoplasia of the hippocampus and incomplete corpus callosum [23, 24], in olfactory neurogenesis [27], and in induction of adipose tissue [28, 29]. Mechanistically, literature to date has focused on physical interactions between Zfp423 and other transcription factors. Alternative levels of integration, such as alterations to cellular signaling centers, have not been well explored.

Hildebrandt and co-workers identified mutations in human *ZNF423* among patients with ciliopathy diagnoses [30]. Patients from all three *ZNF423* families had cerebellar vermis hypoplasia or Joubert Syndrome, while two also had nephronophthisis and other clinical features. Cellular assays with patient mutations showed effects on proliferation and DNA damage response, presenting a new pathogenic mechanism in ciliopathy disorders, but did not assess cilium structure or function. This raises the question of whether *ZNF423* and *Zfp423* mutations phenocopy ciliopathies by acting on downstream signaling events or represent bona fide ciliopathies by affecting cilium function upstream of signaling.

Results here provide new insights into Zfp423-dependent developmental mechanisms. Distinctly different models have been proposed for the cerebellar hypoplasia in *Zfp423* mice and, by extension, human patients. Based on *Zfp423* gene-trap expression in postnatal Purkinje cells, one group proposed a non-autonomous mechanism mediated by diminished Shh production [25], as seen in some Purkinje cell-selective mutations [31]. In situ hybridization, however, showed *Zfp423* expression in both the ventricular zone and the external germinal layer (EGL) in developing cerebellum, equally consistent with a GCP-intrinsic mechanism [23, 24]. We show that GCPs express Zfp423 protein in situ and in primary culture, that loss of Zfp423 blocked their ability to respond to Shh, altered cilium morphologies, decreased Smoothened translocation, and increased expression of several cilium-related genes, including *Tulp3*. Reversing the Tulp3 overexpression restored Smoothened translocation. Our results

105 demonstrate a GCP-intrinsic role for Zfp423 upstream of Shh signaling and suggest
106 excess Tulp3 as a potential target to restore function in ZNF423/Zfp423-deficient cells.
107
108 **RESULTS**

109 ***Zfp423* is expressed in granule cell precursors.**

110 In situ hybridization had previously shown *Zfp423* RNA expression in ventricular
111 zone, external germinal layer and rhombic lip [23, 24], while lacZ reporter expression in
112 a gene trap line suggested expression restricted to Purkinje cells [25], leading to
113 different proposals for developmental defects in mutant embryos. To resolve which cells
114 express Zfp423 in developing cerebellum, we examined Zfp423 protein expression and
115 RNA in isolated cell populations (Fig 1). Zfp423 immunoreactivity showed strong,
116 nuclear-limited signal in postmitotic Purkinje cells and most migrating GCPs in the
117 rhombic lip and external germinal layer (EGL), with somewhat less intense staining in a
118 fraction of ventricular zone cells (Fig 1A). Comparing sections from control (+/+) and
119 *Zfp423* null mutant (*nur12*) congenic littermates that were processed in parallel on single
120 slides demonstrated both specificity and sensitivity of the signal. Similar results have
121 been obtained with two additional, independent antibodies developed against Zfp423 or
122 its human ortholog (L. Flores-García and B.A.H.). As a further test of cell type
123 distribution, we monitored by reverse transcription and quantitative polymerase chain
124 reaction (RT-qPCR) the expression of *Zfp423* and several cell-type selective markers in
125 cerebellar cells isolated by Percoll gradient centrifugation at E18.5 (Fig 1B,C). These
126 data indicated that highly enriched GCP cultures retain *Zfp423* expression while losing
127 Purkinje cell selective markers such as *Rora* and *Shh*. Furthermore, RT-qPCR
128 experiments for expression of *Shh*, the primary mitogen for GCPs, was not significantly
129 different between *Zfp423*-mutant and control cerebellum among several independent

130 samples (Fig 1D). These experiments demonstrate nuclear Zfp423 expression in GCPs
131 in situ, with continued expression in primary culture, and support the potential for a cell-
132 intrinsic role for Zfp423 in the granule cell deficits seen in *Zfp423*$^{-/-}$ animals.
133

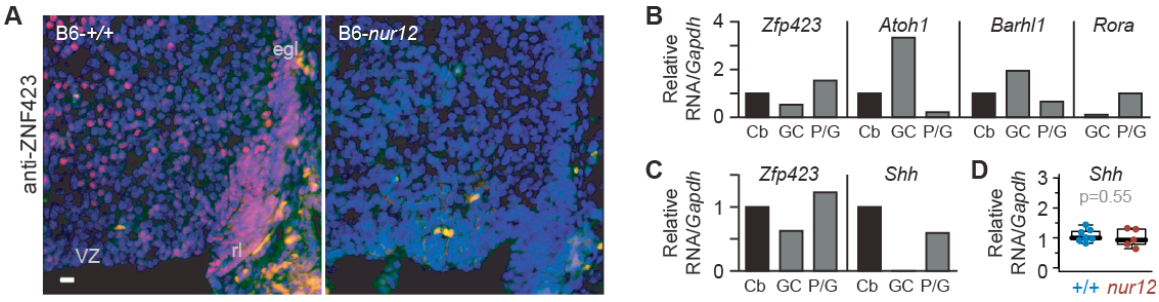

134

135 **Fig 1. Zfp423 is expressed in cerebellar granule cell precursors.** (***A***) Antibody
136 staining at E16.5 shows nuclear expression of Zfp423 in cells of the rhombic lip (rl) and
137 external germinal layer (egl), as well as ventricular zone (VZ) derivatives in control, but
138 not in *Zfp423*^{nur12} mutant cerebellum. (***B***) E18.5 granule cell precursors purified by
139 Percoll gradient centrifugation retain *Zfp423* expression. Quantitative RT-PCR shows co-
140 expression of *Zfp423* with granule-specific *Atoh1* and *Barhl1* RNAs, with loss of Purkinje
141 cell marker *Rora*. Histogram shows average expression ratio among technical replicates
142 from a single purification, normalized to *Gapdh* and expressed relative to whole
143 cerebellum. Cb, whole cerebellum; GC, granule cell/precursor fraction; P/G, Purkinje cell
144 and Glial fraction. Rora level expressed relative to P/G fraction; Cb fraction not run. (***C***)
145 Quantitative RT-PCR with hydrolysis probes (TaqMan) assays shows enrichment of
146 *Zfp423* in the granule cell precursor fraction of a second independent purification. In
147 contrast, no amplification from the granule cell preparation is detected for *Shh*, a GCP
148 mitogen expressed by Purkinje cells. (***D***) RT-qPCR for *Shh* expression in whole
149 cerebellum from control and *nur12* mutant animals dissected on P3. Mean values from
150 technical replicates were normalized to *Gapdh* and expressed as a fraction of a control
151 sample for 7 control and 5 mutant embryos. Similar results were obtained when

normalized to *Ppia* cyclophilin. Group means were not significantly different (p=0.55, t-test).

Zfp423 is required for ex vivo proliferation and Shh responsiveness.

To test whether GCP-intrinsic *Zfp423* expression is relevant to their proliferation phenotype, we transfected purified GCPs with shRNA vectors (Fig 2) that we previously validated for reducing Zfp423 levels [32]. Transfected GCPs were identified by fluorescence of an enhanced green fluorescent protein (EGFP) reporter in the vector. Cells entering S phase were marked by BrdU incorporation (A). The proportion of $EGFP^+$ cells that were also $BrdU^+$ was taken as a mitotic index specific for transfected cells. As predicted from *Zfp423* mutant animals [23], shRNA significantly reduced this index relative to the corresponding index of non-transfected ($EGFP^-$) cells in the same cultures (p = 0.040-0.0014, paired *t* tests) and to approximately one-third the level of cells transfected by empty vector, irrelevant target (luciferase), or scrambled sequence shRNA controls (Fig 2B; $p<10^{-7}$, one-factor ANOVA with post-hoc Tukey HSD test). Because the transfection efficiency in primary GCPs is modest (~15%), most transfected cells were surrounded by non-transfected cells. This minimizes the likelihood of any confounding effects secondary to disrupted cell interactions. These data show that *Zfp423* has a cell-intrinsic effect on GCP proliferation ex vivo and suggest that the effect might be cell autonomous within a population of GCPs, as proliferation phenotype does not appear to depend on the status of adjacent cells in the culture.

Because previous reports have shown that Shh is the principle mitogen for GCP proliferation in vivo and in culture, with a wide dynamic range, we next tested whether Zfp423-depletion in GCPs might alter the dose-response curve for exogenous Shh treatment (Fig 2C). We exposed Zfp423-knockdown and control GCPs to a range of 0-10 µg/ml recombinant Shh concentrations and measured the resulting mitotic index for

178 replicate cultures at each concentration. Two-factor ANOVA on resulting cell count data
179 showed significant impacts of Shh dose ($p = 2.0 \times 10^{-4}$), Zfp423 vs. control shRNA ($p = 9.3 \times 10^{-10}$), and the interaction between dose and shRNA ($p = 6.4 \times 10^{-6}$). Remarkably,
181 Zfp423-shRNA cells were refractory to Shh levels more than an order of magnitude
182 greater than that required to stimulate proliferation of control-shRNA cells. These results
183 indicate a Zfp423-dependent step critical to Shh signal transduction in GCPs.
184

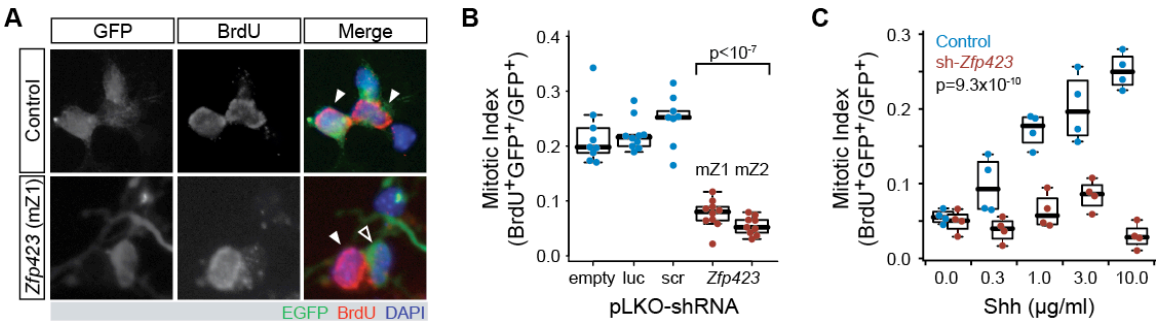

185

186 **Fig 2. *Zfp423* shRNA blocks proliferation and Shh response of purified granule cell**
187 **precursors.** (***A***) Examples of GCPs transfected with scrambled control or *Zfp423*-
188 targeted shRNA constructs, in the presence of 3 µg/ml Shh. Transfected cells express
189 EGFP from the shRNA vector (green). Proliferating cells are labeled by BrdU
190 incorporation for 6 hr, 48 hr after transfection (red). Control panels show dividing
191 transfected cells (closed arrowheads) and a non-dividing, non-transfected, cell (open
192 arrowhead). *Zfp423* (shRNA mZ1) panels show a dividing non-transfected cell (closed
193 arrowhead) and a non-diving transfected cell (open arrowhead). At least two
194 transfections for each of three independent DNA preparations were assayed for each
195 construct. Channel levels were adjusted for merged images. (***B***) The proportion of
196 $EGFP^+$ cells labeled by BrdU is plotted for each replicate culture. shRNA sequence was
197 highly significant ($p < 2.2 \times 10^{-16}$, ANOVA), with each *Zfp423* shRNA construct different
198 from every control ($p < 10^{-7}$ for each pair-wise comparison, Tukey HSD). Controls were

not significantly different from each other ($p > 0.4$), nor were the two *Zfp423* hairpin sequences ($p > 0.4$). Empty, pLKO vector with no hairpin sequence; luc, luciferase; scr, scrambled sequence control; mZ1 and mZ2 are non-overlapping shRNA sequences designed against *Zfp423* from the RNAi consortium collection. (***C***) GCP cultures were transfected with control (scr) or *Zfp423*-targeted (mZ1) shRNA constructs and treated with 0-10 µg/ml Shh. Transfected cells were recognized by EGFP fluorescence, replicating cells by BrdU incorporation. Plotted points indicate mitotic index of transfected cells for each of four replicate experiments at each of the indicated Shh concentrations. A minimum of three independent DNA preparations was used for transfection in each condition. The effect of *Zfp423*-targeting shRNA, Shh concentration, and the interaction between hairpin identity and Shh concentration were each strongly supported statistically ($p= 9.3 \times 10^{-10}$, 2.0×10^{-4}, and 6.4×10^{-6} respectively, two-factor ANOVA).

Zfp423-deficient precursors have abnormal cilium morphology

Because Shh signaling is transduced through components localized to the primary cilium, we next asked whether Zfp423-deficient GCPs made cilia and basal bodies in normal frequency and quality (Fig 3). Cerebellum sections from E18.5 mice showed both structures intact among cells in the EGL and with comparable frequency per cell between *Zfp423*^{nur12}-homozygous and littermate controls by double label immunofluorescence for acetylated α-tubulin (Ac-αTub) in the cilium and γ-tubulin (γTub) in the basal body (Fig 3A). Volume measurements extracted from optical sections, however, showed a significant increase in cilium volume in *Zfp423*^{nur12} EGL compared to littermate controls (Fig 3B). As replicate measurements did not follow a normal distribution within or between biological samples, we made several assessments using non-parametric tests. Among co-processed sections from eight littermate pairs, average

volumes were larger in the mutant than in the control animal for all eight comparisons ($p = 0.0078$, Wilcoxon signed rank test, two tailed). The distribution of volumes between genotypes for all 499 discrete measurements irrespective of pairing was also highly significant ($p = 8.7 \times 10^{-6}$, Kolmogorov-Smirnov test). Mutant cilia also had substantially higher variance than those in control littermates (0.89 vs. 0.33; $p = 1.3 \times 10^{-4}$, Ansari-Bradley test). Similar analysis of basal bodies (Fig 3C) did not support a difference in paired sample averages ($p = 1$), but did support a slightly lower distribution of basal body volumes over 662 individual measurements irrespective of pairs ($p = 0.031$) without significant difference in variances ($p = 0.19$). Mean voxel values for acetylated α-tubulin were 1.02 in control, 1.37 in mutant sections. Mean voxel values for γ-tubulin were 1.35 in control, 1.11 in mutant sections.

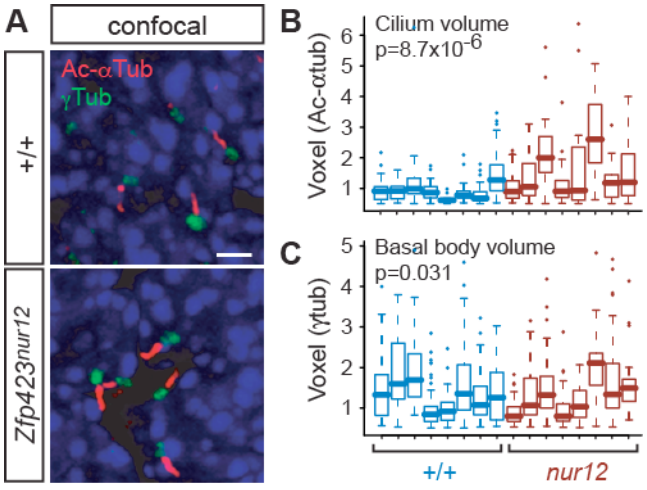

Fig 3. Confocal images show altered primary cilium volumes in *Zfp423^{nur12}* EGL. (***A***) Confocal micrographs show representative projection images showing ciliary axoneme (anti-acetylated α-tubulin, Ac-αTub) and basal bodies (anti-γ-tubulin, γTub) in sections of E18.5 cerebellum from animals of the indicated *Zfp423* genotypes. All images are from sagittal sections, 0.7-0.9 mm from the midline. Scale bar, 2 μm. (***B,C***) Measured volumes for each of 499 axonemes (***B***) and 662 basal bodies (***C***) identified by

the Velocity program from reconstructed optical sections. Measurements from paired mutant and control animals are color coded in the scatter plot. The differences in overall distributions between mutant and control are significant for both axonemes ($p = 8.7 \times 10^{-6}$) and basal bodies ($p = 0.031$, Kolmogorov-Smirnov test) in pooled data from eight pairs of animals.

To understand better the structural basis for these volume differences, we measured discrete parameters by structured illumination "super-resolution" microscopy of cilia from mutant and control littermate animals (Fig 4). We obtained similar results using either Ac-αTub (Fig 4A-C) or Arl13b (Fig 4D-F) as a marker protein. In Ac-αTub measurements, mutant cilia tended to be longer (Fig 4B), though this effect did not reach conventional significance ($p = 0.079$, Wilcoxon rank sum test, two tails), and mutant cilia had a significantly wider base compared with control (Fig 4C, $p = 0.0091$). Structured illumination measurements for Arl13b, associated with the ciliary membrane, showed significant increases in both length (Fig 4E, $p=0.028$) and width (Fig 4F, $p=0.013$) of GCP cilia in an independent set of animals. Taken together, these observations indicate a cellular basis for ciliopathy-related phenotypes of *Zfp423*-deficient mice.

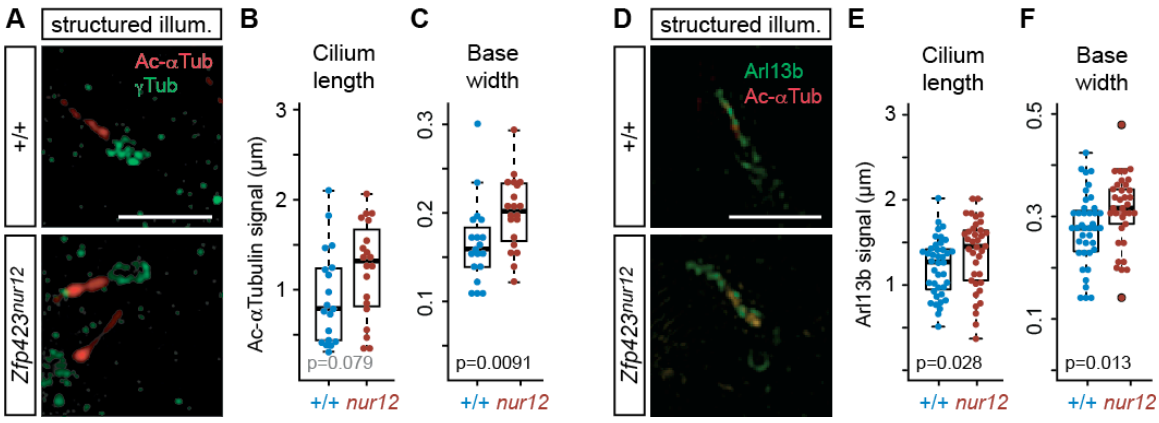

Fig 4. Structured illumination microscopy shows altered cilium dimensions in *Zfp423*^{nur12} EGL. (***A***) Super-resolution images show axoneme (Ac-αTub) and basal body (γTub). Scale bar, 2 μm. (***B,C***) Box and scatter plots show distributions of cilium length (***B***) and base width (***C***) measurements. Significance was assessed from paired samples. Length, p = 0.079, base width p = 0.0091, Wilcoxon rank sum test with two tails. (***D***) Structured illumination micrographs of cilia in the EGL. Arl13b and γ-tubulin in green, acetylated α-tubulin in red. (***E***) Length measurements from Arl13b signal in consecutively imaged cilia showed a shift toward longer axonemes in *nur12* (p = 0.028, Wilcoxon rank sum test). (***F***) Width of the axoneme base was also increased in *nur12* (p = 0.013, Wilcoxon rank sum test).

ZNF423 is required for quantitative Smoothened translocation during Shh signaling

Because Zfp423 is required for Shh response and affected the distribution of cilium morphologies, we asked whether it also affected trafficking of Smoothened, using a cell culture model (Fig 5). DAOY is a human medulloblastoma-derived cell line that expresses markers consistent with a GCP lineage [33, 34] and *ZNF423*, the human homologue of *Zfp423* (Fig 5A). DAOY cells were infected with a pseudotyped lentivirus expressing both a Smoothened-enhanced green fluorescent protein (EGFP) fusion protein and shRNA to either human *ZNF423* or a non-targeting control (Fig 5B). Cells were examined after serum starvation to produce a high percentage of cells with a definitive primary cilium. Two non-overlapping *ZNF423* shRNA were each effective in reducing its level of expression relative to multiple controls, a representative image is shown in Fig 5C. Quantification of fluorescence Western blots showed that, relative to control shRNAs, *ZNF423* knockdown cultures expressed ~30% ZNF423, ~110%

acetylated α-tubulin, and ~95% IFT88 levels scaled to either GAPDH or β-actin as internal loading controls. We then tested the effect of ZNF423 knockdown on Smoothened translocation. Infected DAOY cells were treated with 0.1 µg/ml Shh as a low dose sufficient for signaling [1]. Cells were fixed 6 hr after stimulation and processed for immunofluorescence to visualize localization of the EGFP tag on Smoothened and acetylated α-tubulin as a marker of cilium location. Only $EGFP^+$ cells were included to avoid measurements from uninfected cells. To compare localization of Smoothened-EGFP relative to acetylated α-tubulin, immunofluorescence micrographs (Fig 5D) presented in randomized order were assessed categorically by five observers blinded to experimental conditions, for >800 cilia across five independent experiments. Summary results (Fig 5E) showed significantly less Smoothened-EGFP translocation in *ZNF423*-depleted cells ($1.2x10^{-13}$, chi-square test). Results showed significant differences in each independent experiment ($p = 0.0058$ to $2.9x10^{-5}$).

Mean fluorescence intensities along the length of each cilium were also calculated from the raw image files as a second analytical approach to the same experiments. Cilium annotations and measurements were performed blind to treatment group on images in randomized order. ZNF423-depleted cells showed ~30% reduction in both mean and median Smoothened-EGFP intensities in cilia, with a highly significant population shift between shRNA groups ($p=7.0x10^{-11}$, Wilcoxon rank sum test; each of five replicates was independently significant, $p<0.025$). Ratios of Smoothened-EGFP to acetylated α-tubulin showed even stronger difference between groups ($p<2.2x10^{-16}$), owing to an increase in acetylated α-tubulin signal in knockdown cells. These results strongly support a ZNF423-dependent step in Shh signaling upstream of Smoothened translocation in human DAOY cells.

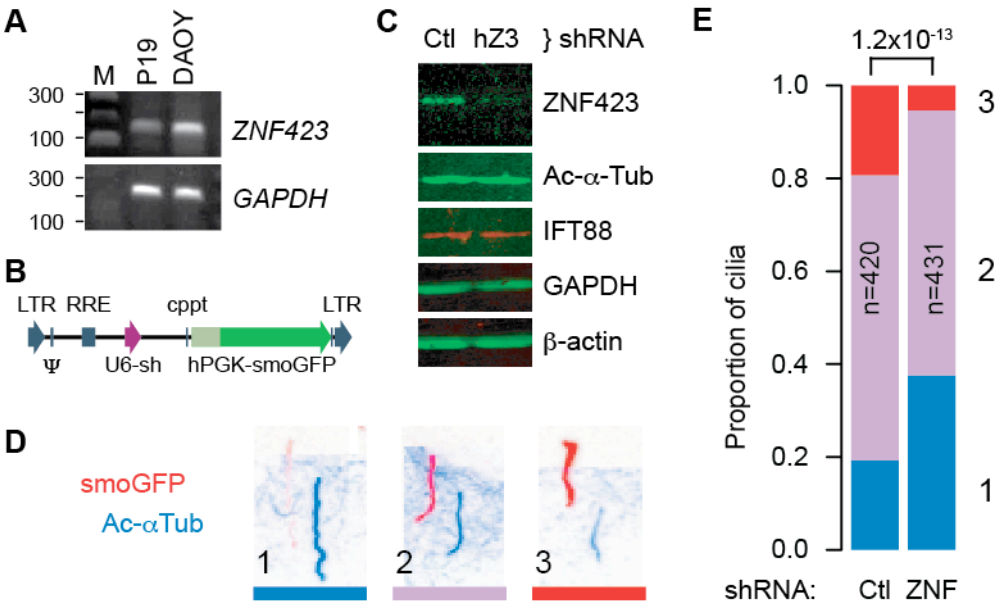

Fig 5. *ZNF423* knockdown quantitatively alters *Smoothened* translocation. (***A***) RT-PCR shows *Zfp423* expression in mouse P19 cells [32] and *ZNF423* RNA expression in DAOY medulloblastoma cells. *GAPDH* was used as a positive control. (***B***) Structure of pLKO-derived lentivirus constructs, expressing a shRNA from a U6 promoter (purple arrow) and Smoothened-EGFP fusion (smoGFP, dark green) from a human *PGK* promoter (light green). Vector backbone elements are indicated in blue. (***C***) Western blots show reduced expression of ZNF423 protein in DAOY infected with lentivirus expressing a *ZNF423* shRNA (hZ3) relative to control (Ctl). (***D***) Color-inverted images of immunofluorescence for both GFP (red) and acetylated a-tubulin (blue) show Smoothened translocation phenotypes of cells infected with lentivirus expressing both smoGFP and an shRNA. Channel layers were shifted diagonally to allow independent view of each. Three categorical phenotypes were observed, (1) strong acetylated α-tubulin with little to no detected Smoothened, (2) intermediate levels, or (3) stronger Smoothened signal relative to acetylated α-tubulin. (***E***) Stacked histogram of cilium phenotypes summarizes five replicate experiments. Phenotypes are color-coded and numbered as in (D). Number of cilia scored in each group (n), *ZNF423*-directed (ZNF) or

control (Ctl) shRNAs, and chi-square p-value for the difference between groups are indicated.

ZNF423 deficiency reduces IFT88 translocation into cilia.

Because Smoothened is thought to use the intraflagellar transport (IFT) system for translocation into cilia [35, 36], we tested whether IFT88 translocation was affected by loss of *ZNF423* in the DAOY culture model or *Zfp423* mutation in vivo (Fig 6). IFT88 is an essential component of the IFT-B complex required for quantitative hedgehog signaling in mice [11] and important for cerebellum development [37]. DAOY cells were infected with viruses described in Fig 5B and selected for cilium expression of the EGFP marker by direct fluorescence after fixation and staining. This necessarily restricted the analysis to the subpopulation of cells with strong Smoothened-EGFP translocation, as direct fluorescence is less sensitive than antibody staining and ZNF423-knockdown cells had a higher proportion of cilia near the detection limit. Among these cells, those transduced with *ZNF423*-directed shRNA showed both increased acetylated α-tubulin intensity relative to control (as predicted by Figures 4 and 5) and dramatically decreased ciliary IFT88 intensity (Fig 6A). The differences between *ZNF423* and control shRNAs reached very high statistical significance for both mean intensities and ratios in cilia (Fig 6B-E, $p<2.2x10^{-16}$, Kruskal-Wallis and Wilcoxon rank sum tests for full and pair-wise comparisons, respectively, in each measure), despite similar overall IFT88 protein levels in cellular extracts after *ZNF423* knockdown, as shown in Fig 5C. Strikingly, the IFT88 signal was also reduced relative to Smoothened-EGFP signal in *ZNF423*-knockdown cells compared to control (Fig 6E), suggesting that loss of IFT88 staining was not a consequence of selection for the high Smoothened-EGFP population or comparison to acetylated α-tubulin levels.

To determine whether similar conditions affect granule precursor cells in situ, we examined the relative distributions of IFT88 and acetylated α-tubulin in the EGL of *Zfp423*^{nur12} and control littermate mice (Fig 6F-G). While most cilia from control littermates showed robust IFT88 staining in the cilium, many cilia in mutant EGL had little or no detectable IFT88 (Fig 6F). The proportion of cilia with little or no IFT88 staining was approximately three times greater among mutant animals than among their control littermates (Fig 6G). Similarly, the overall intensity of IFT88 within the cilium was significantly reduced in GCPs within the EGL of *nur12* animals compared with littermate controls (Fig 6H). Both measures showed highly significant *Zfp423*-dependence across five littermate pairs ($p=3.7 \times 10^{-8}$ for proportion, chi-square test; $p=2.2 \times 10^{-15}$ for signal intensities, Wilcoxon rank sum test with continuity correction). IFT88 translocation thus appears impaired both in the human DAOY cell culture model and in mouse granule cell precursors in tissue sections, providing a proximate cause for diminished Shh signaling both ex vivo and in situ.

Fig 6. Reduced frequency and intensity of axonemal IFT88 in Zfp423-deificent cells. (***A***) Confocal micrographs of DAOY cells transduced with the indicated shRNA and Smoothened-EGFP. Immunofluorescence for acetylated α-tubulin and IFT88 and direct fluorescence of EGFP in representative images are shown. Scale bar, 5 μm. Distributions of mean axonemal measurements for (***B***) acetylated α-tubulin intensity, (***C***) IFT88 intensity, (***D***) ratio of IFT88 to acetylated α-tubulin and (***E***) ratio of IFT88 to Smoothened-EGFP fluorescence across three independent experiments with each shRNA in DAOY cells are plotted. For each plot, differences are highly significant among shRNA treatments ($p<2.2 \times 10^{-16}$, Kruskal-Wallis test) and between the 6 *ZNF423* and control populations ($p<2.2 \times 10^{-16}$, Wilcoxon rank sum test with continuity correction).

(***F***) Confocal images of GCP cilia from EGL of control littermate and *Zfp423* null mutant (*nur12*) mice. Scale bar, 2 µm. (***G***) Localization of IFT88 relative to acetylated α-tubulin in cilia from five littermate pairs shows a lower proportion of mutant cilia with IFT88 throughout the axoneme; $p=3.7x10^{-8}$, chi-square test. (***H***) Mean axonemal intensities of IFT88 are significantly reduced compared to littermate controls. Differences between each littermate pair were independently significant. Difference between genotypes for summed data of 5 pairs is highly significant ($p=2.2x10^{-15}$, Wilcoxon rank sum test).

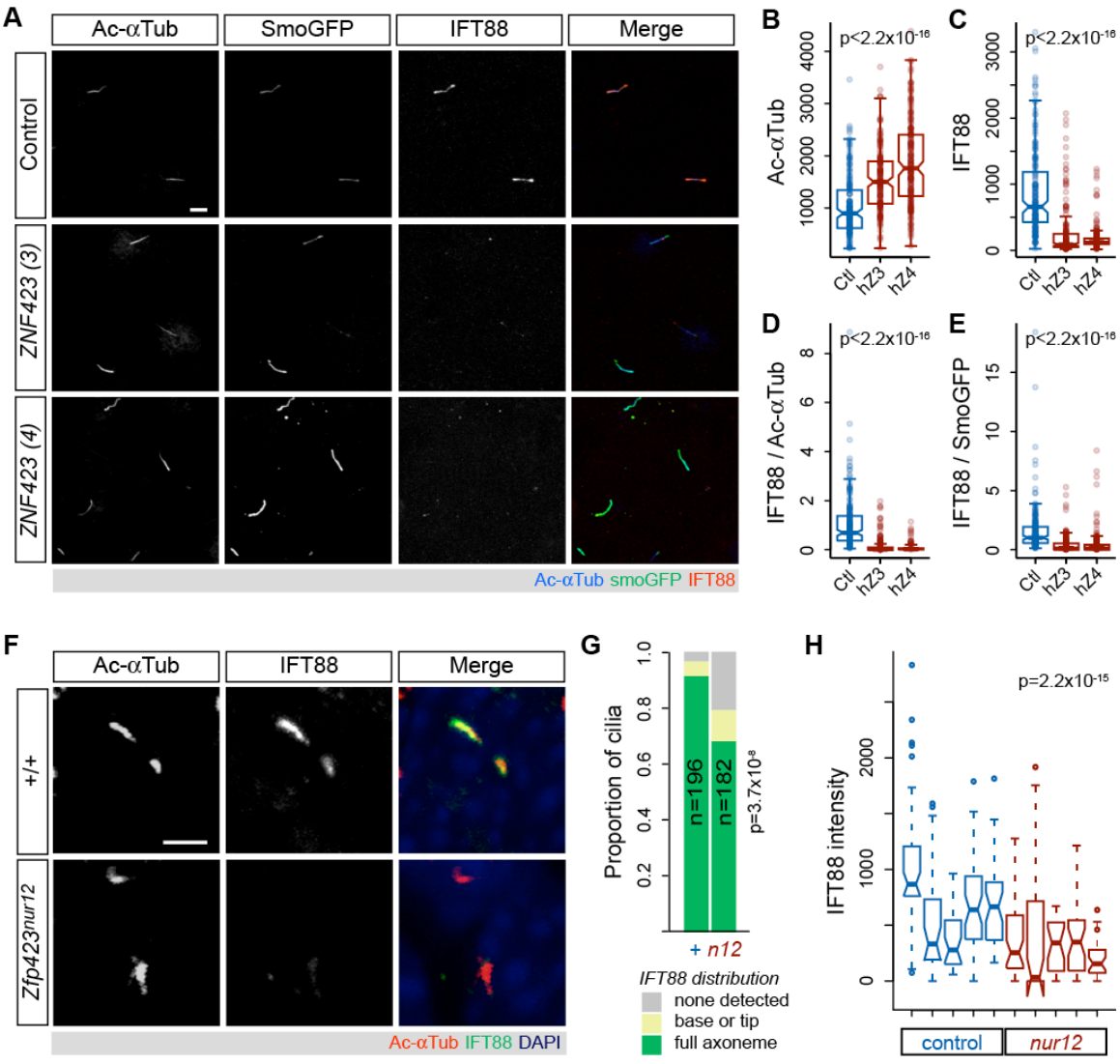

TULP3 overexpression is a functional target of *ZNF423* depletion.

To link the functional requirement for human ZNF423 and mouse Zfp423 to potential target genes required for Shh response via cilia, we performed high-throughput cDNA sequencing (RNA-Seq) on the DAOY cell model, followed by confirmation of specific genes in freshly isolated mouse GCPs (Fig 7). RNA-Seq data were processed for normalized counts of annotated genes and then assessed for significant differences between *ZNF423* and control knockdown samples in three biological replicates, using tools in the HOMER software package [38, 39]. Gene set enrichment analysis [40, 41] did not identify any highly enriched pathways, but showed a strong relationship to genes up-regulated in DAOY cells after knockdown of *PCGF2*, a polycomb repressor complex protein [42]. Of >1000 genes that passed this initial threshold, 12 stood out for their known roles in primary cilia (Fig 7A). To determine whether these differences were conserved between the human medulloblastoma cell line model and mouse GCPs, we measured expression of mouse orthologs to five genes that had FDR < 0.01 and clean assays by RT-qPCR using freshly isolated GCPs from *Zfp423*^{nur12} and littermate controls (Fig 7B). *Tulp3*, *Nek9*, and *Arl4d* showed significantly elevated expression in mutant GCPs, as predicted by the DAOY cell knockdown model, while the other two were not significantly different between genotypes. In both DAOY and GCP cells, *TULP3*/*Tulp3* showed the most significant difference, being overexpressed >2-fold in each context.

A

Gene	Fold change	P-value	FDR	Rank
TULP3	2.16	3.3E-16	3E-13	31
WDR34	0.55	2.0E-11	7E-09	61
CEP170B	0.68	1.5E-05	0.001	331
NEK9	1.33	3.8E-05	0.002	395
FKBP8	0.76	9.4E-05	0.004	475
IFT70	2.59	1.0E-04	0.005	487
ARL4D	2.11	1.2E-04	0.004	501
WNT5A	0.71	3.7E-04	0.011	651
IFT25	1.73	5.6E-04	0.016	720
CILD18	0.78	1.0E-03	0.026	832
JBTS13	1.53	1.1E-03	0.026	833
GLI1	2.01	1.9E-03	0.039	1016

B

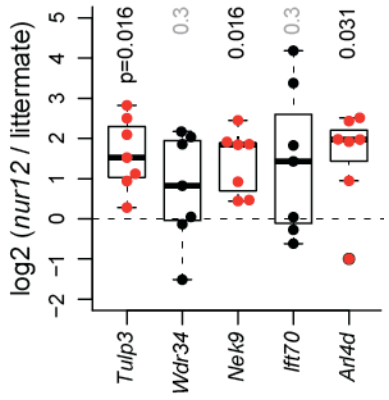

Fig 7. Tulp3 is an expression target of Zfp423 deficiency. (***A***) RNA-Seq data from knockdown and control DAOY cells identified several canonical cilium genes at high confidence. *TULP3* was among the largest magnitude changes and highest statistical confidence. (***B***) RT-qPCR from acutely isolated GCPs confirmed significantly increased expression of *Tulp3*, *Nek9*, and *Arl4d* in mutant relative to non-mutant controls among 7 littermate pairs. Nonparametric p-values from the Wilcoxon signed rank test are shown.

Chromatin immunoprecipitation (ChIP) experiments with independent antibodies demonstrated physical interaction of Zfp423 with the *Tulp3* gene in GCPs. Previous ChIP experiments quantified by high-throughput sequencing (ChIP-Seq) from a P19 cell culture model that expressed high levels of Zfp423, provided only modest read depth relative to cell number [32]. However, these data provided suggestive support for binding ~7 kb 5' to *Arl4d* (Fig 8A) and for sites within and around *Tulp3* (Fig 8B). Because of the low yield in ChIP-Seq experiments and desire to test biological replicate samples, we quantified ChIP at these candidate sites relative to a previously described marker locus, 259C14S [43, 44], by ChIP-qPCR. Both a commercial antibody (goat) and a custom, affinity-purified antibody (rabbit) were previously characterized by Western blotting and immunofluorescence [32]. Both antibodies supported ChIP enrichment of a site in *Tulp3* intron 1 (Tulp3_3) that also had the strongest support in the previous ChIP-Seq data (Fig 8C). Although enrichment over background was modest with the commercial antibody, it was also uniquely significant at the Tulp3_3 site ($p=0.037$, Tukey Honest Significant Difference test after one-factor ANOVA). Enrichment with the custom antibody showed stronger support for the same site ($p=0.012$) and a non-significant trend at the Tulp3_2 site ($p=0.28$). Non-parametric analysis of pooled data from both antibodies supported the same result ($p=0.0087$, Wilcoxon rank sum test for Tulp3_3 vs. control site after Bonferroni correction, with no other pairwise combination $p>0.2$). Neither antibody

showed enrichment for the other two candidate sites. Taken together, six independent ChIP experiments from primary GCPs support a direct and selective physical association of Zfp423 with sequences in *Tulp3* intron 1.

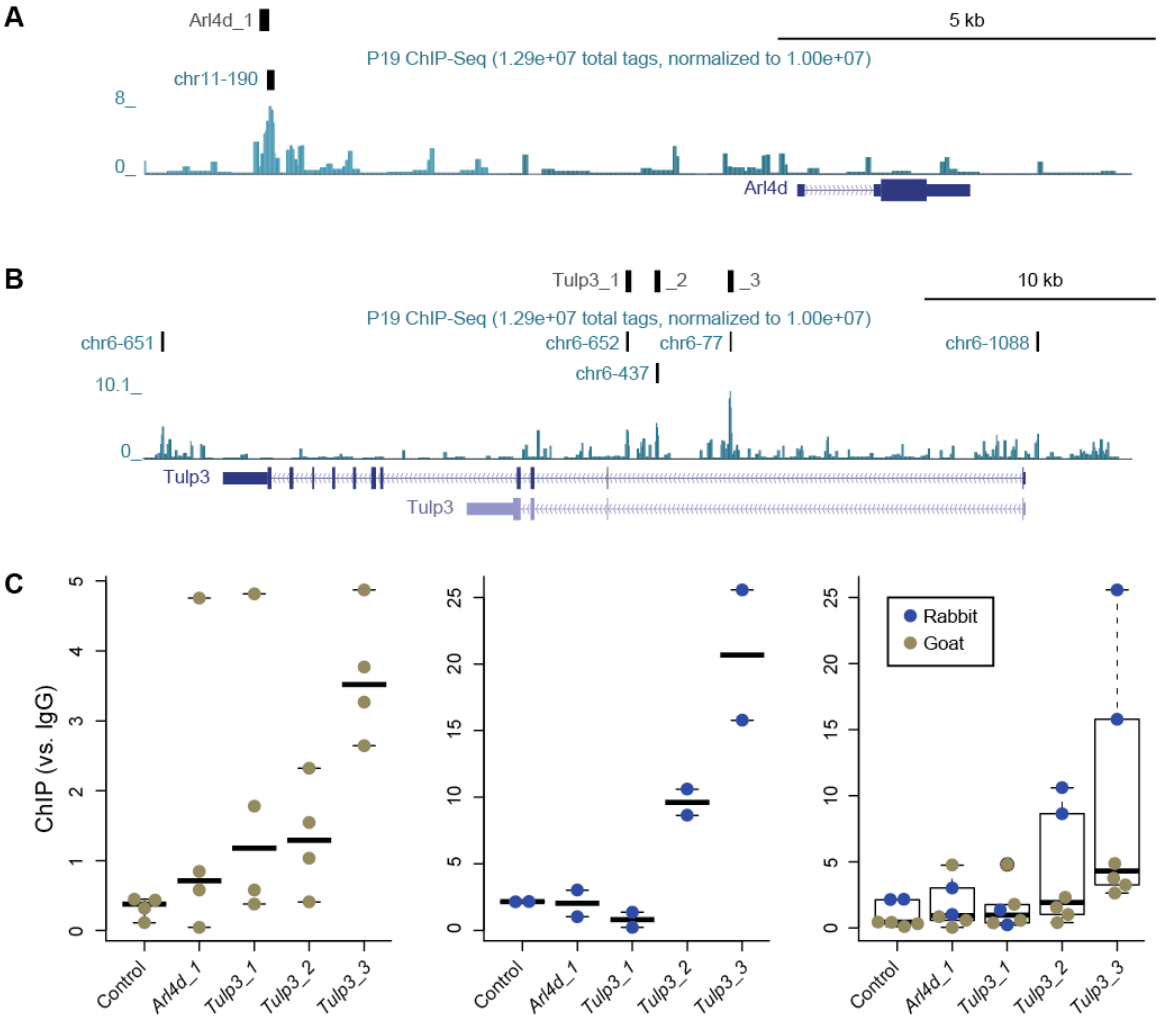

Fig 8. Chromatin immunoprecipitation detects Zfp423 binding in *Tulp3* intron 1. (***A***) UCSC browser window on *Arl4d* locus shows location of the ChIP-PCR assay (Arl4d_1) and a ChIP-Seq peak call from P19 cells (chr11-190), 7 kb 5' to the annotated transcript (Arl4d). The peak notation indicates the 190th best-supported peak on chromosome 11 in that experiment [32]. (***B***) Similar window on *Tulp3* locus includes 5 potential peaks from P19 ChIP-Seq data, three of which supported reliable quantitative PCR assays

(Tulp3_1, _2 and _3) within 150 bp of the peak. (***C***) Graphs show fold enrichment relative to an IgG control for a control locus and the four candidate binding sites. Colored dots indicate measured values from independent biological replicates, bars indicate median values for each locus. A commercial anti-Zfp423 antibody developed in goat (blue dots) showed modest but significant enrichment for Tulp3_3. A custom antibody developed in rabbit and affinity purified against the immunogen showed strong enrichment for Tulp3_3 and possible enrichment for Tulp3_2, 3 kb away. Non-parametric analysis of the combined data provides strong and conservative statistical support for binding at Tulp3_3 (p=0.0087, Wilcoxon rank sum test with Bonferroni correction).

To test the functional importance of TULP3 overexpression in effecting ZNF423 depletion phenotype, we compared knockdown of *ZNF423* to simultaneous knockdown of both *ZNF423* and *TULP3.* Combinations of targeting or control shRNAs were delivered to DAOY cells using lentiviral vectors. Knockdown of *ZNF423* with either of two non-overlapping shRNA depleted ZNF423 protein to ~50% of control levels (by Western blot) and produced ~2-fold increase in TULP3 protein in each culture (Fig 9A), even though only 60-75% cells appeared to be productively infected based on the fluorescent reporter protein. Of three shRNAs directed against *TULP3*, only T2 and T3 were effective in reducing measured TULP3 protein level (Fig 9B). T2 and T3 reduced TULP3 levels in *ZNF423*-knockdown cells to 70-90% of levels in control cells with full ZNF423 expression. We then compared Smoothened-GFP translocation in doubly-infected cells, with ~100 cilia per group in two independent experiments (Fig 9C), following the methods and scoring described for *ZNF423* knockdown in Fig 5. Simultaneous knockdown of *TULP3* significantly reversed the reduction in Smoothened-GFP translocation caused by knockdown *ZNF423* in each replicate experiment (p=0.0023 - 6.2x10-5, Pearson's chi-squared test, 2 degrees of freedom for high vs. low

473 TULP3). Each of the effective *TULP3* shRNAs showed similar result on Smoothened-
474 GFP distribution. These results indicate a functional role for TULP3 overexpression in
475 mediating defective signaling in the primary cilium of ZNF423-deficient cells.
476

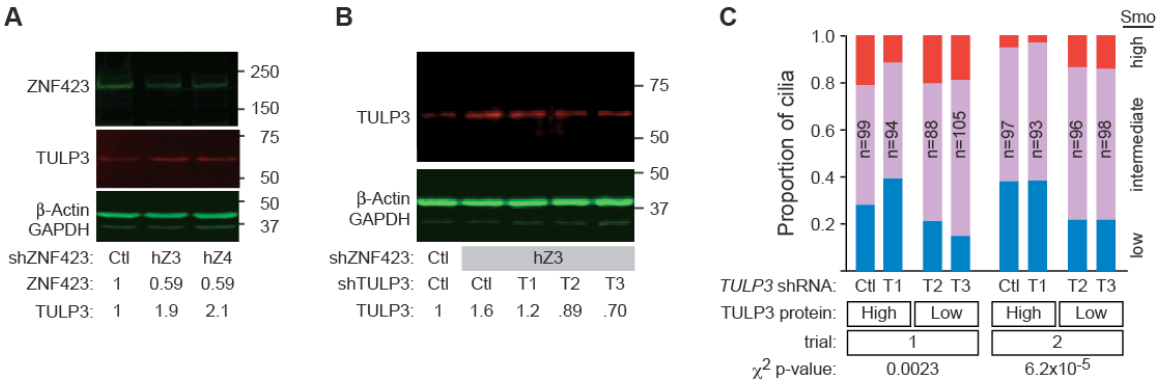

477

478 **Fig 9. Tulp3 is a functional target of Zfp423.** (***A***) Western blot shows loss of ZNF423
479 and increase of TULP3 levels in DAOY cells infected with lentiviral shRNA vectors
480 targeting *ZNF423*. Relative amounts are compared to control shRNA infections after
481 normalization to β-actin and GAPDH. (***B***) Western blot shows the effect of dual infection
482 by *ZNF423* and three independent *TULP3* shRNA vectors on TULP3 protein. Only
483 shRNAs T2 and T3 reduced TULP3 levels compared with control vector. (***C***) Co-infection
484 with *ZNF423* and *TULP3* shRNA reverses the decrease in Shh-stimulated Smoothened
485 GFP translocation into cilia seen with shRNA to *ZNF423* and either scrambled control or
486 an ineffective *TULP3* shRNA. Graphs indicate high (red), medium (purple) and low
487 (blue) translocation as in Fig 5D,E. Chi-square
488

489 **DISCUSSION**

490 Our work provides, in both mouse brain and human cell culture models, the first
491 mechanistic connection between ZNF423/Zfp423 ciliopathy-related phenotypes and
492 function of the primary cilium. While phenotype severity and range of organ involvement

493 vary, cerebellar vermis hypoplasia is a uniquely consistent feature among reported
494 *ZNF423* families [30] and five *Zfp423* mouse mutations on a variety of strain
495 backgrounds [23-26]. Previous work in mice demonstrated loss of precursor proliferation
496 [23], though the site of action has remained unresolved between competing proposals
497 for cell intrinsic (potentially cell-autonomous) mechanisms in the granule cell lineage and
498 non-autonomous mechanisms through Shh expression in Purkinje cells. Analysis of cell
499 culture models previously uncovered defective DNA damage response as a novel
500 cellular mechanism in *ZNF423* patient-derived mutations [30], but did not assess effects
501 on primary cilia and left open the question of whether ZNF423 might also act upstream
502 of the cilium to regulate its function or downstream by mitigating its effects. Results
503 presented here demonstrate a role for human and mouse homologs in cilium function
504 and in intrinsic properties of granule cell precursors, acting – at least in part – through
505 elevated expression of TULP3. Our work further unites cilium function and DNA damage
506 response mechanisms by demonstrating that defects in both can occur through
507 mutations for the same molecular component.

508 Four lines of evidence implicate *Zfp423* as a bona fide ciliopathy gene. First,
509 both recessive loss of function and apparently dominant mutations in mice and humans
510 produce phenotypes within the ciliopathy spectrum, including cerebellar vermis
511 hypoplasia in both species, nephronophthisis in humans, and a variable degree of other
512 consequences that may reflect allele strength or genetic, environmental or stochastic
513 modifiers [23, 24, 26, 30]. Second, our imaging analyses show that while *Zfp423*-null
514 animals make primary cilia at a normal frequency, loss of Zfp423 results in an abnormal
515 distribution of morphologies. Cilia on mutant GCPs, as a group, appear wider near the
516 base (Fig 3 and Fig 4), where several Joubert Syndrome and nephronophthisis proteins
517 are localized [45-48], and tend to be longer. Structures at the base act to regulate traffic
518 of signaling cargoes into and out of the cilium [49, 50]. This striking difference in cilium

519 morphologies could be explained by an altered temporal profile of dynamic states, as the
520 ranges of measurements largely overlap between genotypes despite having different
521 distributions. Third, signaling through the primary cilium is functionally defective after
522 loss of Zfp423 activity. *Zfp423*-depleted primary GCPs are refractory to exogenous Shh
523 (Fig 2). *ZNF423*-depleted DAOY medulloblastoma cells are reproducibly deficient in
524 translocation into the cilium of both Smoothened (Fig 5) and IFT88 (Fig 6), which are
525 required for normal signal processing [12, 13, 51-53] and specifically for expansion of
526 GCPs [15]. Diminished IFT88 translocation was also seen in mouse GCPs in situ (Fig
527 6). Fourth, we find expression level changes in key cilium components that are
528 consistent between *ZNF423*-knockdown DAOY cells and *Zfp423*-mutant GCPs and
529 indicative of disrupted signaling, at least one of which is functionally important and likely
530 due to direct regulation. TULP3 was the best-supported target of Zfp423 in our analysis.
531 TULP3 is an inhibitor of Shh signaling and loss of *Tulp3* in mice results in increased Shh
532 signaling [54-56]. At a cellular level, TULP3 regulates ciliary trafficking at both retrograde
533 transport and cilium entry through its interaction with IFT-A [57, 58]. ChIP experiments
534 in primary GCPs with two different antibodies against Zfp423 both showed significant
535 enrichment of a site in *Tulp3* intron 1 that was predicted from an earlier analysis in a P19
536 cell culture model [32]. Functionally, reversing the overexpression of TULP3 caused by
537 ZNF423 depletion significantly reversed the Smoothened translocation defects of
538 *ZNF423* knockdown cells (Fig 9).

539 Although Zfp423 is required for mitogenic response to Shh ex vivo, residual
540 proliferation both in knockdown cells and in the EGL of null animals away from the
541 midline shows that Zfp423 is not strictly required for all mitogenic response by GCPs.
542 Moreover, the DAOY model shows residual translocation of both IFT88 and
543 Smoothened-EGFP in knockdown cells. One possibility might be that mitogenic
544 response by GCPs is more sensitive to loss of *Zfp423* when cultured ex vivo than either

545 GCPs in situ or the transformed DAOY model–and it is not unreasonable to expect that
546 both environmental factors and intrinsic cell differences relevant to establishment of a
547 cell line might enhance proliferative response. Alternatively (or additionally), it may be
548 that IFT-independent diffusion of Smoothened into the cilium [50] provides a modest
549 level of signaling that is saturated at lower levels of Shh than the translocation-
550 dependent pathway, as might be suggested by the difference in sensitivity of
551 Smoothened-EGFP and IFT88 localization to DAOY cell cilia (Fig 6E).

552 Tulp3 overexpression may be a surprising candidate for limiting Smoothened
553 translocation. Although Tulp3 antagonizes Shh signaling, loss of *Tulp3* does not affect
554 Smoothened trafficking [57, 59]. Rather, Tulp3 is thought to inhibit Shh signaling through
555 localization of Gpr161, whose activation elevates cAMP level to promote cleavage of Gli
556 proteins to their repressor forms [58]. However, this well-documented mechanism is
557 based on Tulp3 loss-of-function may not be the only inhibitory effect when Tulp3 is
558 expressed substantially above its normal level, as in ZNF423/Zfp423 deficient cells (Fig
559 7 and 9). Excess Tulp3 could in principle recruit additional inhibitory molecules to the
560 cilium or titrate limiting components that promote Smoothened trafficking, such as
561 Gprasp2 or Pifo [60, 61]. It is also possible that excess Tulp3 affects cell state in a way
562 that indirectly affects IFT88 and Smoothened translocation to or concentration in the
563 primary cilium. More work is needed to test such hypotheses, which are not mutually
564 exclusive. In addition, since Zfp423 contributes to regulation of several ciliopathy-related
565 genes, the full extent of molecular consequences is likely to be more complex and
566 interplay among dysregulated components may be required to fully resolve molecular
567 mechanisms behind the anatomical phenotypes seen in both patients and mouse
568 models.

569 Our results have some similarities to those with ciliogenic transcription factors of
570 the RFX family and Foxj1 [62, 63], but also important differences. RFX proteins are

571 highly conserved regulators that activate core components for formation of motile cilia
572 and loss of RFX activity results in loss or truncation of cilia [64-68]. *Foxj1* is a Shh target
573 gene that also activates components for motile cilia and is sufficient to drive ciliogenesis,
574 though loss of *Foxj1* does not generally prevent cilium formation [69, 70]. Restoring
575 expression of target genes partially mitigates cell phenotypes [71]. By contrast, *ZNF423*
576 patients and *Zfp423* mouse models present phenotypes more typical of defects in non-
577 motile cilia, especially cerebellum vermis hypoplasia [23, 24, 30] and Zfp423 is not
578 required for appearance of cilia. Zfp423 is required for efficient signaling through cilia in
579 cerebellum and in the cell models we tested. Zfp423 appears to modulate components,
580 often as a negative regulator and we see improvement of cell phenotypes by mitigating
581 the overexpression of the first clear repression target, *TULP3*, in a DAOY cell model.
582 The results here demonstrate a signaling mechanism, complementary to the
583 DNA damage response (DDR) mechanism demonstrated by Chaki et al. [30], for
584 neurodevelopmental phenotypes in *ZNF423*-deficient patients and orthologous *Zfp423*
585 mutant mice. In addition to providing a structural and functional basis for diminished Shh
586 signaling in granule cell precursors, our results point to loss of Zfp423 repressive
587 functions on *Tulp3* and potentially other genes as a key component of the phenotype.
588 Establishment of both DDR and signaling mechanisms provides a more comprehensive
589 basis for understanding both the variety and variability of disease presentations in this
590 ciliopathy, and potentially in others.

591

592 **MATERIALS AND METHODS**

593 *Mice*. The *nur12* mutation and BALB/c–*Zfp423*^{nur12} and C57BL/6–*Zfp423*^{nur12} congenic
594 mice have been previously described [23, 26, 72]. For timed matings, midnight on the

night of conception was considered to be E0.0. All procedures were approved by the UC San Diego Institutional Animal Care and Use Committee.

Antibodies. Anti-BrdU antibody (mouse monoclonal B44) was purchased from BD Biosciences. anti-GFP antibody (A11122) purchased from Molecular Probes. Antibodies against acetylated α-tubulin (mouse monoclonal 6-11B-1, T6793) and γ-tubulin (rabbit polyclonal, T5192) were purchased from Sigma-Aldrich. Rabbit anti-IFT88 (13967-1-AP), TULP3 (13637-1-AP), and Arl13b (17711-1-AP) were purchased from Proteintech. Mouse anti-GAPDH antibody (GT239) was purchased from GeneTex. Rabbit antiserum against Human ZNF423 (amino acid residues 247-407 relative to reference sequence NP_055884.2), was prepared and affinity-purified against the immunogen [32]. Commercial antibodies against ZNF423 (Santa Cruz Biotechnology sc-48785, aa 1-105; Sigma-Aldrich SAB2104426, aa 1234-1283) showed similar pattern (L. Flores-Garcia and B.A.H.). Western blots were developed with infrared-conjugated secondary antibodies (Rockland), detected on a Li-Cor Odyssey Imaging Station, and quantified in the ImageJ software package.

Primary cell culture and mitotic index. Primary GCPs were isolated from E18.5 cerebella of BALB/c mice by Percoll gradient centrifugation essentially as described [73, 74], but omitting the adhesion step. Transfection experiments were performed with a minimum of three independent DNA preparations for each construct. 48 hrs after transfection, cells were exposed to 4 μg/ml BrdU (Sigma-Aldrich) for 6 hrs prior to fixation with 4% paraformaldehyde. Recombinant Shh was purchased from R&D Systems. TRC shRNAs 708 and 709 directed against mouse *Zfp423* were obtained from Sigma (Table 1).

620 *Gene expression assays.* Quantitative RT-PCR was carried out on a Bio-Rad CFX-96
621 using SYBR Green fluorescence as described [43]. TaqMan hydrolysis probe assays
622 (Life Technologies; *Shh* assay Mm00436528_m1, *Zfp423* assay Mm00473699_m1,
623 *Gapdh* assay 4352339E.) were performed on the same instrument, following
624 manufacturer's recommended conditions. Relative quantification used the $\Delta\Delta C_T$ method
625 and comparisons across isolated cell fractions were expressed relative to the same ratio
626 in whole cerebellum.
627
628 *Immunofluorescence and cilium measurements.* For tissues, 10 μm sections were
629 prepared from 4% paraformaldehyde fixed animals at age E18.5. Confocal (Olympus
630 FV1000) and structured illumination "super resolution" microscopy (Applied Precision
631 OMX) were performed in the UCSD School of Medicine Light Microscopy Facility.
632 Volume measurements on the acquired images were accessed by Volocity software
633 (PerkinElmer). For Smoothened translocation measurements, a Smoothened-EGFP
634 fusion gene [75] was obtained from Addgene and cloned into pLKO.1 vector (Sigma),
635 along with shRNA constructs targeting either *ZNF423*, scrambled control, or irrelevant
636 sequence controls directed against reporter genes not used in this study. Human
637 medulloblastoma-derived DAOY cells were obtained from Dr. Robert Wechsler-Reya.
638 TRC shRNA directed against human *ZNF423* were obtained from Sigma (Table 1).
639 Virus particles were packaged by co-transfection of 293FT cells with pCMVdR8.2 dvpr
640 and pCMV-VSV-G (Addgene plasmid 8455 and 8454) as described [76]. Replicate
641 cultures of DAOY cells were infected with each virus for 5 hr., cultured 7 days and serum
642 starved for 24 hr prior to treatment with 0.1 μg/ml Shh for 24 hrs. Cells were fixed in 4%
643 paraformaldehyde and imaged by confocal microscopy. Sixty-two to 100 consecutive
644 images were collected for each sample and images from paired samples randomly
645 ordered (knockdown vs. control) into a grid by the flip of a coin. Distribution of

646 Smoothened-GFP relative to acetylated α-tubulin was assessed as a nominal-scale
647 variable by 5 different investigators blinded to genotype and experimental condition.
648 Mean Intensity along the axoneme of each channel was measured by ImageJ (National
649 Institute of Health, USA).
650
651 *RNA-seq*
652 ZNF423 knockdown and control DAOY cells were generated with a modified pLKO
653 lentivirus that expressed shRNA to ZNF423 or a non targeting control and co-expressed
654 the fluorescent protein mCherry. Cells expressing high level of mCherry were enriched
655 by flow cytometry and cultured in three replicate plates per virus. Bar-coded RNA
656 libraries were prepared for sequencing using strand specific dUTP protocols [39] with
657 minor modifications. Briefly, total RNA was harvested using Trizol reagent. Poly(A) +
658 RNA was enriched with Dynabeads® mRNA Purification Kit (Life Technologies,
659 Cat#61006). For each library, 500 ng poly(A) + RNA was premixed with 0.2 µg of
660 Oligo(dT) and random hexamer primer, heated to 70 °C for 10 min., and chilled on ice.
661 Reverse transcription reactions were incubated at room temperature for 10 min., 42 °C
662 1h and 50 °C 20 min. First-strand cDNA was ethanol precipitated with 0.5 volumes 5 M
663 ammonium acetate. After second-strand cDNA synthesis, sequencing libraries were
664 constructed as described [38]. 250 to 500 bp size-selected, adaptor-ligated cDNA was
665 incubated with 1 U USER (NEB) at 37 °C for 15 min. followed by 5 min. at 95 °C before
666 PCR with Phusion High-Fidelity DNA polymerase. High-throughput sequencing was
667 performed by UCSD IGM Genomics Center. Reads were aligned to the human hg19
668 transcriptome using STAR version 2.3.1f [77]. Data analysis was performed using
669 HOMER [38] and the Bioconductor package edgeR [78, 79]. Gene set enrichment was
670 performed in GSEA [40, 41]
671

672 *Chromatin Immunoprecipitation*. ChIP was performed as described [32]. Briefly, 5-10 x
673 10^6 purified primary GCPs were crosslinked in 1% formaldehyde, sonicated, and
674 subjected to standard ChIP purification with the indicated antibodies at ~2 µg.
675 Quantitative PCR from ChIP samples used 0.5% input fraction and ChIP with pre-
676 immune IgG for relative quantification among samples.
677
678 *Statistical tests.* Standard statistical procedures were performed in the R base
679 environment (R 2.8.1 GUI 1.27 Tiger build 32-bit (5301)). Normality (Shapiro-Wilk test)
680 and equal variance (F test) of each data set was assessed prior to selecting parametric
681 (ANOVA, *t*) or non-parametric (Kruskal-Wallis, Wilcoxon) tests. Tukey box-and-whisker
682 plots indicate median (heavy line), quartile (box), and 1.5 times interquartile range
683 (whiskers). Notches where shown indicate ±1.58 times the interquartile range/square
684 root of *n*.
685

686 **ACCESSION NUMBERS**

687 RNA-seq data have been submitted and can be accessed by the Gene Expression
688 Omnibus (GEO) accession number GSE59598.
689

690 **ACKNOWLEDGEMENTS**

691 The authors gratefully acknowledge Robert Wechsler-Reya for DAOY cells, Young-
692 Wook Cho for affinity-purified ZNF423 antibody, Wendy Alcaraz, Dorothy Concepcion,
693 Lisbeth Flores-Garcia, Kevin Ross, Isabella Sanchez, Weica Xie, and Susan Zhang for
694 manual scoring of de-identified images, Jennifer Santini of the UCSD Neuroscience
695 Microscopy Shared Facility for advice and assistance with instrumentation, Sven Heinz
696 and Christopher K. Glass for advice on RNA-Seq library preparation and HOMER
697 software, the UCSD Institute for Genomic Medicine Genomics Core for high-throughput
698 sequencing and Lawrence S. B. Goldstein and Xiang-Dong Fu for comments on draft
699 manuscripts. The authors declare no competing financial interests.

700

REFERENCES

1. Wechsler-Reya RJ, Scott MP. Control of neuronal precursor proliferation in the cerebellum by Sonic Hedgehog. Neuron. 1999;22(1):103-14. PubMed PMID: 10027293.

2. Wallace VA. Purkinje-cell-derived Sonic hedgehog regulates granule neuron precursor cell proliferation in the developing mouse cerebellum. Curr Biol. 1999;9(8):445-8. PubMed PMID: 10226030.

3. Dahmane N, Ruiz-i-Altaba A. Sonic hedgehog regulates the growth and patterning of the cerebellum. Development. 1999;126(14):3089-100. PubMed PMID: 10375501.

4. Corrales JD, Blaess S, Mahoney EM, Joyner AL. The level of sonic hedgehog signaling regulates the complexity of cerebellar foliation. Development. 2006;133(9):1811-21. Epub 2006/03/31. doi: 10.1242/dev.02351. PubMed PMID: 16571625.

5. Marino S. Medulloblastoma: developmental mechanisms out of control. Trends Mol Med. 2005;11(1):17-22. Epub 2005/01/15. doi: 10.1016/j.molmed.2004.11.008. PubMed PMID: 15649818.

6. Roussel MF, Hatten ME. Cerebellum development and medulloblastoma. Curr Top Dev Biol. 2011;94:235-82. Epub 2011/02/08. doi: 10.1016/B978-0-12-380916-2.00008-5. PubMed PMID: 21295689.

7. Wechsler-Reya R, Scott MP. The developmental biology of brain tumors. Annu Rev Neurosci. 2001;24:385-428. PubMed PMID: 11283316.

8. Stanton BZ, Peng LF. Small-molecule modulators of the Sonic Hedgehog signaling pathway. Mol Biosyst. 2010;6(1):44-54. Epub 2009/12/22. doi: 10.1039/b910196a. PubMed PMID: 20024066.

9. Hyman JM, Firestone AJ, Heine VM, Zhao Y, Ocasio CA, Han K, et al. Small-molecule inhibitors reveal multiple strategies for Hedgehog pathway blockade. Proc Natl Acad Sci U S A. 2009;106(33):14132-7. Epub 2009/08/12. doi: 10.1073/pnas.0907134106. PubMed PMID: 19666565; PubMed Central PMCID: PMC2721821.

10. Romer J, Curran T. Targeting medulloblastoma: small-molecule inhibitors of the Sonic Hedgehog pathway as potential cancer therapeutics. Cancer Res. 2005;65(12):4975-8. Epub 2005/06/17. doi: 10.1158/0008-5472.CAN-05-0481. PubMed PMID: 15958535.

11. Huangfu D, Liu A, Rakeman AS, Murcia NS, Niswander L, Anderson KV. Hedgehog signalling in the mouse requires intraflagellar transport proteins. Nature. 2003;426(6962):83-7. Epub 2003/11/07. doi: 10.1038/nature02061. PubMed PMID: 14603322.

12. Corbit KC, Aanstad P, Singla V, Norman AR, Stainier DY, Reiter JF. Vertebrate Smoothened functions at the primary cilium. Nature. 2005;437(7061):1018-21. Epub 2005/09/02. doi: 10.1038/nature04117. PubMed PMID: 16136078.

13. Haycraft CJ, Banizs B, Aydin-Son Y, Zhang Q, Michaud EJ, Yoder BK. Gli2 and Gli3 localize to cilia and require the intraflagellar transport protein polaris for processing and function. PLoS Genet. 2005;1(4):e53. Epub 2005/10/29. doi: 10.1371/journal.pgen.0010053. PubMed PMID: 16254602; PubMed Central PMCID: PMC1270009.

14. Huangfu D, Anderson KV. Cilia and Hedgehog responsiveness in the mouse. Proc Natl Acad Sci U S A. 2005;102(32):11325-30. Epub 2005/08/03. doi: 10.1073/pnas.0505328102. PubMed PMID: 16061793; PubMed Central PMCID: PMC1183606.

15. Spassky N, Han YG, Aguilar A, Strehl L, Besse L, Laclef C, et al. Primary cilia are required for cerebellar development and Shh-dependent expansion of progenitor pool. Dev Biol. 2008;317(1):246-59. Epub 2008/03/21. doi: 10.1016/j.ydbio.2008.02.026. PubMed PMID: 18353302.

16. Tsai RY, Reed RR. Cloning and functional characterization of Roaz, a zinc finger protein that interacts with O/E-1 to regulate gene expression: implications for olfactory neuronal development. J Neurosci. 1997;17(11):4159-69. PubMed PMID: 9151733.

17. Hata A, Seoane J, Lagna G, Montalvo E, Hemmati-Brivanlou A, Massague J. OAZ uses distinct DNA- and protein-binding zinc fingers in separate BMP-Smad and Olf signaling pathways. Cell. 2000;100(2):229-40. PubMed PMID: 10660046.

18. Ku MC, Stewart S, Hata A. Poly(ADP-ribose) polymerase 1 interacts with OAZ and regulates BMP-target genes. Biochem Biophys Res Commun. 2003;311(3):702-7. PubMed PMID: 14623329.

19. Holzel M, Huang S, Koster J, Ora I, Lakeman A, Caron H, et al. NF1 is a tumor suppressor in neuroblastoma that determines retinoic acid response and disease outcome. Cell. 2010;142(2):218-29. Epub 2010/07/27. doi: 10.1016/j.cell.2010.06.004. PubMed PMID: 20655465; PubMed Central PMCID: PMC2913027.

20. Huang S, Laoukili J, Epping MT, Koster J, Holzel M, Westerman BA, et al. ZNF423 is critically required for retinoic acid-induced differentiation and is a marker of neuroblastoma outcome. Cancer Cell. 2009;15(4):328-40. PubMed PMID: 19345331.

21. Masserdotti G, Badaloni A, Green YS, Croci L, Barili V, Bergamini G, et al. ZFP423 coordinates Notch and bone morphogenetic protein signaling, selectively up-regulating Hes5 gene expression. J Biol Chem. 2010;285(40):30814-24. PubMed PMID: 20547764.

22. Signaroldi E, Laise P, Cristofanon S, Brancaccio A, Reisoli E, Atashpaz S, et al. Polycomb dysregulation in gliomagenesis targets a Zfp423-dependent differentiation network. Nat Commun. 2016;7:10753. Epub 2016/03/01. doi: 10.1038/ncomms10753. PubMed PMID: 26923714; PubMed Central PMCID: PMC4773478.

778 23. Alcaraz WA, Gold DA, Raponi E, Gent PM, Concepcion D, Hamilton BA. Zfp423
779 controls proliferation and differentiation of neural precursors in cerebellar vermis
780 formation. Proc Natl Acad Sci U S A. 2006;103(51):19424-9. PubMed PMID: 17151198.

781 24. Cheng LE, Zhang J, Reed RR. The transcription factor Zfp423/OAZ is required
782 for cerebellar development and CNS midline patterning. Dev Biol. 2007;307(1):43-52.
783 PubMed PMID: 17524391.

784 25. Warming S, Rachel RA, Jenkins NA, Copeland NG. Zfp423 is required for normal
785 cerebellar development. Mol Cell Biol. 2006;26(18):6913-22. PubMed PMID: 16943432.

786 26. Alcaraz WA, Chen E, Valdes P, Kim E, Lo YH, Vo J, et al. Modifier genes and
787 non-genetic factors reshape anatomical deficits in Zfp423-deficient mice. Hum Mol
788 Genet. 2011;20(19):3822-30. Epub 2011/07/07. doi: 10.1093/hmg/ddr300. PubMed
789 PMID: 21729880; PubMed Central PMCID: PMC3168291.

790 27. Cheng LE, Reed RR. Zfp423/OAZ participates in a developmental switch during
791 olfactory neurogenesis. Neuron. 2007;54(4):547-57. PubMed PMID: 17521568.

792 28. Gupta RK, Arany Z, Seale P, Mepani RJ, Ye L, Conroe HM, et al. Transcriptional
793 control of preadipocyte determination by Zfp423. Nature. 2010;464(7288):619-23.
794 PubMed PMID: 20200519.

795 29. Zhang LJ, Guerrero-Juarez CF, Hata T, Bapat SP, Ramos R, Plikus MV, et al.
796 Innate immunity. Dermal adipocytes protect against invasive Staphylococcus aureus
797 skin infection. Science. 2015;347(6217):67-71. Epub 2015/01/03. doi:
798 10.1126/science.1260972. PubMed PMID: 25554785; PubMed Central PMCID:
799 PMC4318537.

800 30. Chaki M, Airik R, Ghosh AK, Giles RH, Chen R, Slaats GG, et al. Exome Capture
801 Reveals ZNF423 and CEP164 Mutations, Linking Renal Ciliopathies to DNA Damage
802 Response Signaling. Cell. 2012;150(3):533-48. Epub 2012/08/07. doi:
803 10.1016/j.cell.2012.06.028. PubMed PMID: 22863007.

804 31. Gold DA, Baek SH, Schork NJ, Rose DW, Larsen DD, Sachs BD, et al. RORa
805 coordinates reciprocal signaling in cerebellar development through sonic hedgehog and
806 calcium-dependent pathways. Neuron. 2003;40(6):1119-31. PubMed PMID: 14687547.

807 32. Cho YW, Hong CJ, Hou A, Gent PM, Zhang K, Won KJ, et al. Zfp423 binds
808 autoregulatory sites in p19 cell culture model. PloS One. 2013;8(6):e66514. Epub
809 2013/06/14. doi: 10.1371/journal.pone.0066514. PubMed PMID: 23762491; PubMed
810 Central PMCID: PMC3675209.

811 33. Jacobsen PF, Jenkyn DJ, Papadimitriou JM. Establishment of a human
812 medulloblastoma cell line and its heterotransplantation into nude mice. J Neuropathol
813 Exp Neurol. 1985;44(5):472-85. Epub 1985/09/01. PubMed PMID: 2993532.

814 34. Peyrl A, Krapfenbauer K, Slavc I, Yang JW, Strobel T, Lubec G. Protein profiles
815 of medulloblastoma cell lines DAOY and D283: identification of tumor-related proteins
816 and principles. Proteomics. 2003;3(9):1781-800. Epub 2003/09/16. doi:
817 10.1002/pmic.200300460. PubMed PMID: 12973738.

818 35. Wang Y, Zhou Z, Walsh CT, McMahon AP. Selective translocation of intracellular
819 Smoothened to the primary cilium in response to Hedgehog pathway modulation. Proc
820 Natl Acad Sci U S A. 2009;106(8):2623-8. Epub 2009/02/07. doi:
821 10.1073/pnas.0812110106. PubMed PMID: 19196978; PubMed Central PMCID:
822 PMC2650314.

823 36. Kuzhandaivel A, Schultz SW, Alkhori L, Alenius M. Cilia-mediated hedgehog
824 signaling in Drosophila. Cell Rep. 2014;7(3):672-80. Epub 2014/04/29. doi:
825 10.1016/j.celrep.2014.03.052. PubMed PMID: 24768000.

826 37. Chizhikov VV, Davenport J, Zhang Q, Shih EK, Cabello OA, Fuchs JL, et al. Cilia
827 proteins control cerebellar morphogenesis by promoting expansion of the granule
828 progenitor pool. J Neurosci. 2007;27(36):9780-9. Epub 2007/09/07. doi:
829 10.1523/JNEUROSCI.5586-06.2007. PubMed PMID: 17804638.

830 38. Heinz S, Benner C, Spann N, Bertolino E, Lin YC, Laslo P, et al. Simple
831 combinations of lineage-determining transcription factors prime cis-regulatory elements
832 required for macrophage and B cell identities. Mol Cell. 2010;38(4):576-89. Epub
833 2010/06/02. doi: 10.1016/j.molcel.2010.05.004. PubMed PMID: 20513432; PubMed
834 Central PMCID: PMC2898526.

835 39. Levin JZ, Yassour M, Adiconis X, Nusbaum C, Thompson DA, Friedman N, et al.
836 Comprehensive comparative analysis of strand-specific RNA sequencing methods. Nat
837 Methods. 2010;7(9):709-15. Epub 2010/08/17. doi: 10.1038/nmeth.1491. PubMed PMID:
838 20711195; PubMed Central PMCID: PMC3005310.

839 40. Mootha VK, Lindgren CM, Eriksson KF, Subramanian A, Sihag S, Lehar J, et al.
840 PGC-1alpha-responsive genes involved in oxidative phosphorylation are coordinately
841 downregulated in human diabetes. Nat Genet. 2003;34(3):267-73. Epub 2003/06/17. doi:
842 10.1038/ng1180. PubMed PMID: 12808457.

843 41. Subramanian A, Tamayo P, Mootha VK, Mukherjee S, Ebert BL, Gillette MA, et
844 al. Gene set enrichment analysis: a knowledge-based approach for interpreting genome-
845 wide expression profiles. Proc Natl Acad Sci U S A. 2005;102(43):15545-50. Epub
846 2005/10/04. doi: 10.1073/pnas.0506580102. PubMed PMID: 16199517; PubMed Central
847 PMCID: PMC1239896.

848 42. Wiederschain D, Chen L, Johnson B, Bettano K, Jackson D, Taraszka J, et al.
849 Contribution of polycomb homologues Bmi-1 and Mel-18 to medulloblastoma
850 pathogenesis. Mol Cell Biol. 2007;27(13):4968-79. Epub 2007/04/25. doi:
851 10.1128/MCB.02244-06. PubMed PMID: 17452456; PubMed Central PMCID:
852 PMC1951487.

853 43. Concepcion D, Flores-Garcia L, Hamilton BA. Multipotent genetic suppression of
854 retrotransposon-induced mutations by Nxf1 through fine-tuning of alternative splicing.
855 PLoS Genet. 2009;5(5):e1000484. Epub 2009/05/14. doi:
856 10.1371/journal.pgen.1000484. PubMed PMID: 19436707; PubMed Central PMCID:
857 PMC2674570.

858 44. Floyd JA, Gold DA, Concepcion D, Poon TH, Wang X, Keithley E, et al. A natural
859 allele of Nxf1 suppresses retrovirus insertional mutations. Nat Genet. 2003;35(3):221-8.
860 PubMed PMID: 14517553.

861 45. Badano JL, Mitsuma N, Beales PL, Katsanis N. The ciliopathies: an emerging
862 class of human genetic disorders. Annu Rev Genomics Hum Genet. 2006;7:125-48.
863 Epub 2006/05/26. doi: 10.1146/annurev.genom.7.080505.115610. PubMed PMID:
864 16722803.

865 46. Lee JE, Gleeson JG. Cilia in the nervous system: linking cilia function and
866 neurodevelopmental disorders. Curr Opin Neurol. 2011;24(2):98-105. Epub 2011/03/10.
867 doi: 10.1097/WCO.0b013e3283444d05. PubMed PMID: 21386674.

868 47. Louie CM, Gleeson JG. Genetic basis of Joubert syndrome and related disorders
869 of cerebellar development. Hum Mol Genet. 2005;14 Spec No. 2:R235-42. Epub
870 2005/10/26. doi: 10.1093/hmg/ddi264. PubMed PMID: 16244321.

871 48. Wolf MT, Hildebrandt F. Nephronophthisis. Pediatr Nephrol. 2011;26(2):181-94.
872 Epub 2010/07/24. doi: 10.1007/s00467-010-1585-z. PubMed PMID: 20652329.

873 49. Hu Q, Milenkovic L, Jin H, Scott MP, Nachury MV, Spiliotis ET, et al. A septin
874 diffusion barrier at the base of the primary cilium maintains ciliary membrane protein
875 distribution. Science. 2010;329(5990):436-9. Epub 2010/06/19. doi:
876 10.1126/science.1191054. PubMed PMID: 20558667; PubMed Central PMCID:
877 PMC3092790.

878 50. Milenkovic L, Scott MP, Rohatgi R. Lateral transport of Smoothened from the
879 plasma membrane to the membrane of the cilium. J Cell Biol. 2009;187(3):365-74. Epub
880 2009/12/02. doi: 10.1083/jcb.200907126. PubMed PMID: 19948480; PubMed Central
881 PMCID: PMC2779247.

882 51. Liu A, Wang B, Niswander LA. Mouse intraflagellar transport proteins regulate
883 both the activator and repressor functions of Gli transcription factors. Development.
884 2005;132(13):3103-11. Epub 2005/06/03. doi: 10.1242/dev.01894. PubMed PMID:
885 15930098.

886 52. May SR, Ashique AM, Karlen M, Wang B, Shen Y, Zarbalis K, et al. Loss of the
887 retrograde motor for IFT disrupts localization of Smo to cilia and prevents the expression
888 of both activator and repressor functions of Gli. Dev Biol. 2005;287(2):378-89. Epub
889 2005/10/19. doi: 10.1016/j.ydbio.2005.08.050. PubMed PMID: 16229832.

890 53. Caspary T, Larkins CE, Anderson KV. The graded response to Sonic Hedgehog
891 depends on cilia architecture. Dev Cell. 2007;12(5):767-78. Epub 2007/05/10. doi:
892 10.1016/j.devcel.2007.03.004. PubMed PMID: 17488627.

893 54. Cameron DA, Pennimpede T, Petkovich M. Tulp3 is a critical repressor of mouse
894 hedgehog signaling. Dev Dyn. 2009;238(5):1140-9. Epub 2009/04/01. doi:
895 10.1002/dvdy.21926. PubMed PMID: 19334287.

896 55. Norman RX, Ko HW, Huang V, Eun CM, Abler LL, Zhang Z, et al. Tubby-like
897 protein 3 (TULP3) regulates patterning in the mouse embryo through inhibition of

898 Hedgehog signaling. Hum Mol Genet. 2009;18(10):1740-54. Epub 2009/03/17. doi:
899 10.1093/hmg/ddp113. PubMed PMID: 19286674; PubMed Central PMCID:
900 PMC2671991.

901 56. Patterson VL, Damrau C, Paudyal A, Reeve B, Grimes DT, Stewart ME, et al.
902 Mouse hitchhiker mutants have spina bifida, dorso-ventral patterning defects and
903 polydactyly: identification of Tulp3 as a novel negative regulator of the Sonic hedgehog
904 pathway. Hum Mol Genet. 2009;18(10):1719-39. Epub 2009/02/19. doi:
905 10.1093/hmg/ddp075. PubMed PMID: 19223390; PubMed Central PMCID:
906 PMC2671985.

907 57. Mukhopadhyay S, Wen X, Chih B, Nelson CD, Lane WS, Scales SJ, et al.
908 TULP3 bridges the IFT-A complex and membrane phosphoinositides to promote
909 trafficking of G protein-coupled receptors into primary cilia. Genes Dev.
910 2010;24(19):2180-93. Epub 2010/10/05. doi: 10.1101/gad.1966210. PubMed PMID:
911 20889716; PubMed Central PMCID: PMC2947770.

912 58. Mukhopadhyay S, Wen X, Ratti N, Loktev A, Rangell L, Scales SJ, et al. The
913 ciliary G-protein-coupled receptor Gpr161 negatively regulates the Sonic hedgehog
914 pathway via cAMP signaling. Cell. 2013;152(1-2):210-23. Epub 2013/01/22. doi:
915 10.1016/j.cell.2012.12.026. PubMed PMID: 23332756.

916 59. Qin J, Lin Y, Norman RX, Ko HW, Eggenschwiler JT. Intraflagellar transport
917 protein 122 antagonizes Sonic Hedgehog signaling and controls ciliary localization of
918 pathway components. Proc Natl Acad Sci U S A. 2011;108(4):1456-61. Epub
919 2011/01/07. doi: 10.1073/pnas.1011410108. PubMed PMID: 21209331; PubMed Central
920 PMCID: PMC3029728.

921 60. Jung B, Messias AC, Schorpp K, Geerlof A, Schneider G, Saur D, et al. Novel
922 small molecules targeting ciliary transport of Smoothened and oncogenic Hedgehog
923 pathway activation. Sci Rep. 2016;6:22540. Epub 2016/03/05. doi: 10.1038/srep22540.
924 PubMed PMID: 26931153; PubMed Central PMCID: PMC4773810.

925 61. Jung B, Padula D, Burtscher I, Landerer C, Lutter D, Theis F, et al. Pitchfork and
926 Gprasp2 Target Smoothened to the Primary Cilium for Hedgehog Pathway Activation.
927 PLoS One. 2016;11(2):e0149477. Epub 2016/02/24. doi: 10.1371/journal.pone.0149477.
928 PubMed PMID: 26901434; PubMed Central PMCID: PMC4763541.

929 62. Thomas J, Morle L, Soulavie F, Laurencon A, Sagnol S, Durand B.
930 Transcriptional control of genes involved in ciliogenesis: a first step in making cilia. Biol
931 Cell. 2010;102(9):499-513. Epub 2010/08/10. doi: 10.1042/BC20100035. PubMed
932 PMID: 20690903.

933 63. Choksi SP, Lauter G, Swoboda P, Roy S. Switching on cilia: transcriptional
934 networks regulating ciliogenesis. Development. 2014;141(7):1427-41. Epub 2014/03/20.
935 doi: 10.1242/dev.074666. PubMed PMID: 24644260.

936 64. Swoboda P, Adler HT, Thomas JH. The RFX-type transcription factor DAF-19
937 regulates sensory neuron cilium formation in C. elegans. Mol Cell. 2000;5(3):411-21.
938 Epub 2000/07/06. PubMed PMID: 10882127.

939 65. Dubruille R, Laurencon A, Vandaele C, Shishido E, Coulon-Bublex M, Swoboda
940 P, et al. Drosophila regulatory factor X is necessary for ciliated sensory neuron
941 differentiation. Development. 2002;129(23):5487-98. Epub 2002/10/31. PubMed PMID:
942 12403718.

943 66. Bonnafe E, Touka M, AitLounis A, Baas D, Barras E, Ucla C, et al. The
944 transcription factor RFX3 directs nodal cilium development and left-right asymmetry
945 specification. Mol Cell Biol. 2004;24(10):4417-27. Epub 2004/05/04. PubMed PMID:
946 15121860; PubMed Central PMCID: PMC400456.

947 67. Ashique AM, Choe Y, Karlen M, May SR, Phamluong K, Solloway MJ, et al. The
948 Rfx4 transcription factor modulates Shh signaling by regional control of ciliogenesis. Sci
949 Signal. 2009;2(95):ra70. Epub 2009/11/06. doi: 10.1126/scisignal.2000602. PubMed
950 PMID: 19887680.

951 68. Piasecki BP, Burghoorn J, Swoboda P. Regulatory Factor X (RFX)-mediated
952 transcriptional rewiring of ciliary genes in animals. Proc Natl Acad Sci U S A.
953 2010;107(29):12969-74. Epub 2010/07/10. doi: 10.1073/pnas.0914241107. PubMed
954 PMID: 20615967; PubMed Central PMCID: PMC2919930.

955 69. Yu X, Ng CP, Habacher H, Roy S. Foxj1 transcription factors are master
956 regulators of the motile ciliogenic program. Nat Genet. 2008;40(12):1445-53. Epub
957 2008/11/18. doi: 10.1038/ng.263. PubMed PMID: 19011630.

958 70. Cruz C, Ribes V, Kutejova E, Cayuso J, Lawson V, Norris D, et al. Foxj1
959 regulates floor plate cilia architecture and modifies the response of cells to sonic
960 hedgehog signalling. Development. 2010;137(24):4271-82. Epub 2010/11/26. doi:
961 10.1242/dev.051714. PubMed PMID: 21098568; PubMed Central PMCID:
962 PMC2990214.

963 71. Lu H, Toh MT, Narasimhan V, Thamilselvam SK, Choksi SP, Roy S. A function
964 for the Joubert syndrome protein Arl13b in ciliary membrane extension and ciliary length
965 regulation. Dev Biol. 2015;397(2):225-36. Epub 2014/12/03. doi:
966 10.1016/j.ydbio.2014.11.009. PubMed PMID: 25448689.

967 72. Kile BT, Hentges KE, Clark AT, Nakamura H, Salinger AP, Liu B, et al.
968 Functional genetic analysis of mouse chromosome 11. Nature. 2003;425(6953):81-6.
969 PubMed PMID: 12955145.

970 73. Hatten ME. Neuronal regulation of astroglial morphology and proliferation in vitro.
971 J Cell Biol. 1985;100(2):384-96. Epub 1985/02/01. PubMed PMID: 3881455; PubMed
972 Central PMCID: PMC2113456.

973 74. Hatten ME, Gao W-Q, Morrison ME, Mason CA. The Cerebellum: Purification
974 and Coculture of Identified Cell Populations. In: Banker G, Goslin K, editors. Culturing
975 Nerve Cells. 2nd ed. ed. Cambridge, MA: MIT Press; 1998.

976 75. Chen JK, Taipale J, Cooper MK, Beachy PA. Inhibition of Hedgehog signaling by
977 direct binding of cyclopamine to Smoothened. Genes Dev. 2002;16(21):2743-8. Epub
978 2002/11/05. doi: 10.1101/gad.1025302. PubMed PMID: 12414725; PubMed Central
979 PMCID: PMC187469.

980 76. Stewart SA, Dykxhoorn DM, Palliser D, Mizuno H, Yu EY, An DS, et al.
981 Lentivirus-delivered stable gene silencing by RNAi in primary cells. RNA. 2003;9(4):493-
982 501. Epub 2003/03/22. PubMed PMID: 12649500; PubMed Central PMCID:
983 PMC1370415.

984 77. Dobin A, Davis CA, Schlesinger F, Drenkow J, Zaleski C, Jha S, et al. STAR:
985 ultrafast universal RNA-seq aligner. Bioinformatics. 2013;29(1):15-21. Epub 2012/10/30.
986 doi: 10.1093/bioinformatics/bts635. PubMed PMID: 23104886; PubMed Central PMCID:
987 PMC3530905.

988 78. Anders S, McCarthy DJ, Chen Y, Okoniewski M, Smyth GK, Huber W, et al.
989 Count-based differential expression analysis of RNA sequencing data using R and
990 Bioconductor. Nat Protoc. 2013;8(9):1765-86. Epub 2013/08/27. doi:
991 10.1038/nprot.2013.099. PubMed PMID: 23975260.

992 79. Robinson MD, McCarthy DJ, Smyth GK. edgeR: a Bioconductor package for
993 differential expression analysis of digital gene expression data. Bioinformatics.
994 2010;26(1):139-40. Epub 2009/11/17. doi: 10.1093/bioinformatics/btp616. PubMed
995 PMID: 19910308; PubMed Central PMCID: PMC2796818.
996

997

998 **TABLES**

999 Table 1: shRNA sequences

shRNA	Target species	Source	Lab name	Full name	Sequence
mZ1	mouse	TRC/ Sigma	708	TRCN0000 084708	CCGGCCCTGAATGTAACGTGAAGTTCTCGAGAACTTCACGTTA CATTCAGGGTTTTT
mZ2	mouse	TRC/ Sigma	709	TRCN0000 084709	CCGGCGGTGCATTACATGACTACATCTCGAGATGTAGTCATGT AATGCACCGTTTTT
hZ3	human	TRC/ Sigma	8173	TRCN0000 018173	CCGGGCAACGTTTGTTCACGGACTTCTCGAGAAGTCCGTGAAC AAACGTTGCTTTTT
hZ4	human	TRC/ Sigma	8174	TRCN0000 018174	CCGGCCACATGATTGAGGAAGGCATCTCGAGATGCCTTCCTCA ATCATGTGGTTTTT
T1	human	TRC/ Sigma	45	TRCN0000 078045	CCGGCCTACTATATGTACTTGGAAACTCGAGTTTCCAAGTACA TATAGTAGGTTTTT
T2	human	TRC/ Sigma	46	TRCN0000 078046	CCGGCCCAGTCAGCATGTTTAGAAACTCGAGTTTCTAAACATG CTGACTGGGTTTTT
T3	human	TRC/ Sigma	47	TRCN0000 078047	CCGGCCAGTTGATTTATCTCGTGAACTCGAGTTCACGAGATAA ATCAACTGGTTTTT
luc	-	TRC/ Sigma	luc	SHC007	CCGGCGCTGAGTACTTCGAAATGTCCTCGAGGACATTTCGAAG TACTCAGCGTTTTT
scr	-	TRC/ Sigma	non-human or mouse	SHC002	CCGGCAACAAGATGAAGAGCACCAACTCGAGTTGGTGCTCTTC ATCTTGTTGTTTTT

1000